Directly cast fibrous heterostructured $FeNi_{0.9}Cr_{0.5}Al_{0.4}$ high entropy alloy with low-cost and remarkable tensile properties

Zhenfei Jiang [a,b], Weiping Chen [a], Chenliang Chu [a], Zhiqiang Fu [a,*], Julia Ivanisenko [b], Hao Wang [a], Siyuan Peng [a], Yemao Lu [b,*], Enrique J. Lavernia [c], Horst Hahn [b,c]

[a] Guangdong Key Laboratory for Advanced Metallic Materials Processing, South China University of Technology, Guangzhou, Guangdong, 510640, China
[b] Institute of Nanotechnology, Karlsruhe Institute of Technology (KIT), D-76021, Karlsruhe, Germany
[c] Department of Materials Science and Engineering, University of California, Irvine, Irvine, CA, 92697, USA

ARTICLE INFO

Keywords:
Cast
High entropy alloy
Fiber
Heterogeneous
Mechanical properties

ABSTRACT

As-cast alloys generally require additional processing steps before optimal strength-ductility combinations can be achieved, thereby impeding the progress of manufacturing high-performance metallic products by direct casting. Here we report a novel low-cost $FeNi_{0.9}Cr_{0.5}Al_{0.4}$ high entropy alloy with unique fibrous heterogeneous solidification microstructure, i.e., fibers-like face-centered-cubic soft phases that are enveloped in nano-sized ordered body-centered-cubic hard shells. This fibrous microstructure is thought to be responsible for the notable mechanical properties, which includes a yield strength of ~670 MPa and an ultimate tensile strength of ~1196 MPa, together with a uniform elongation of ~21.1% at room temperature. Experimental results confirm the suggestion that the combination of a high strength and good ductility can be attributed to the hetero-deformation induced hardening mechanism generated from the soft-fiber and hard-shell interface. The cost-effectiveness of this as-cast $FeNi_{0.9}Cr_{0.5}Al_{0.4}$ alloy with its unique fibrous structure and outstanding tensile properties renders it an ideal candidate for structural applications.

As an ancient method of manufacturing metallic materials, casting techniques are extensively used to manufacture many types of products, including those with complex geometries [1,2]. The near-net-shape forming capability of casting can significantly reduce the amount of raw material needed and shorten the manufacturing process compared with other subtractive processes, thereby leading to much lower cost, high productivity as well as lower environmental impact [1,2]. Unfortunately, bulk metals prepared by directly cast rarely possess optimal combinations of strength and elongation. The family of high entropy alloys (HEAs) have triggered significant research interest owing to their great potential in enhancing materials' mechanical performance [3–7]. Over the past decade, a wide variety of as-cast HEAs with unconventional microstructures have been designed taking advantage of the design flexibility that this new family of alloys provides. For example, nanometer precipitates-enhanced CoCrCuMnNi HEA has an ultimate tensile strength of 742 MPa with an elongation of 40% at the as-cast condition [8]. Our previous studies on equiatomic AlCrFeNi HEA shows a rare chrysanthemum-like structure and exhibits a high compressive fracture strength with a reasonable strain [9]. Recently, the concept of eutectic HEA (EHEA) was proposed by Lu et al., developing the $AlCoCrFeNi_{2.1}$ HEA, which forms a fine lamellar structure of the soft FCC phase and hard B2 phase, exhibiting an ultimate tensile strength of 1080 ± 23 MPa with elongation of 16.2 ± 0.8 % [10,11]. Nevertheless, reports on HEAs with properties that exceed those of Ni-based superalloys consistently involve chemistries with large amounts of Co which drastically increases cost [5-8,10-12]. The overall combination of a complex process with expensive elemental additions has restricted the use of HEAs in many engineering applications [12].

Therefore, a series of Co-free and/or cost-effective HEAs with various mechanical properties have been developed [12–16]. For instance, the $Fe_{50-x}Ni_{25}Cr_{25}Mo_x$ and $CrFeNiAl_xTi_y$ HEAs are economically competitive and exhibit balanced compression properties in the as-cast state [13,14]. In addition, the thermomechanically processed, metastable $Fe_{50}Mn_{30}Co_{10}Cr_{10}$ HEA exhibits a high elongation of over 70% which was attributed to a transformation-induced plasticity (TRIP) mechanism that is activated during deformation [15]. Moreover, the partially recrystallized $Fe_{35}Ni_{35}Cr_{25}Mo_5$ HEA with heterogeneous lamellar structure shows a tensile strength over 1.1 GPa and a total elongation of

* Corresponding authors.
E-mail addresses: zhiqiangfu2019@scut.edu.cn (Z. Fu), Yemao.Lu@partner.kit.edu (Y. Lu).

~13% [16]. Despite significant research efforts towards the development of low-cost HEAs, the results reported thus far have been underwhelming and only a few Co-free as-cast HEAs with exceptional combinations of gigapascal tensile strength and large ductility have been reported. Typically, single FCC HEAs exhibit commendable ductility but inferior yield strength in their as-cast state [8,12-14], whereas single BCC HEAs possess high strength but albeit with limited ductility at room temperature [11–13]. Hence, the direct casting of alloys with superior mechanical performance is highly desirable for enhancing engineering reliability and energy efficiency.

In this work, we designed a novel Co-free non-equiatomic FeNiCrAl HEA based on a grouping strategy used for the extensively studied $AlCoCrFeNi_{2.1}$ EHEA. According to the previously proposed grouping strategy established on mixing enthalpy [17,18], the elements are divided into two distinct groups; i.e., one is the intermetallic group composed of Al and Ni (with a negative mixing enthalpy of -22 kJ/mol [19]), and the other is the solid solution group composed of Co, Cr, Fe, and Ni (with a mixing enthalpy close to zero [19]). Additionally, a previous study on Al-Mg_2Si-Ni alloy reveals that the lamellar structure can form when the volume fraction of each phase is higher than $1/\pi$ (31.8%), whereas a rod-like structure can form when the volume fraction of one phase is lower than $1/\pi$ [20]. Therefore, a Co-free $FeNi_{0.9}Cr_{0.5}Al_{0.4}$ HEA was designed by reducing the content of the AlNi intermetallic group to $0.9/\pi$ (~28.6%, slightly lower than the critical value), and accordingly the content of CoFeCrNi group was increased to ~71.4%. In the meantime, the high-cost Co was replaced by Fe with the aim of lowering the raw material cost.

The $FeNi_{0.9}Cr_{0.5}Al_{0.4}$ HEA ingot was produced from metal pieces (purity > 99.9 wt.%) utilizing the conventional vacuum arc-melting method under argon protection. The ingot was inverted and remelted four times with electromagnetic stirring to ensure chemical homogeneity. The melted button was subsequently drop-cast into a copper mold with dimensions of 70 × 10 × 10 mm^3 by gravity. The crystalline structure was identified by X-ray diffraction (XRD, X'pert powder, PANalytical) with Cu Kα radiation. The morphology was characterized by a field-emission scanning electron microscope (SEM, Auriga 60, Zeiss) in a backscatter electron (BSE) mode. Further phase identification and elemental distribution were conducted on an aberration-correction transmission electron microscope (TEM, Themis-Z, Thermo Fisher Scientific) equipped with Super-X energy dispersive X-ray spectrometry (EDS). Uniaxial tension test and loading-unloading-reloading (LUR) cyclic tension test with a nominal strain rate of 1×10^{-3} s^{-1} were performed on a universal testing machine (Zwick/Roell Z020) equipped with a mechanical extensometer at room temperature. Three

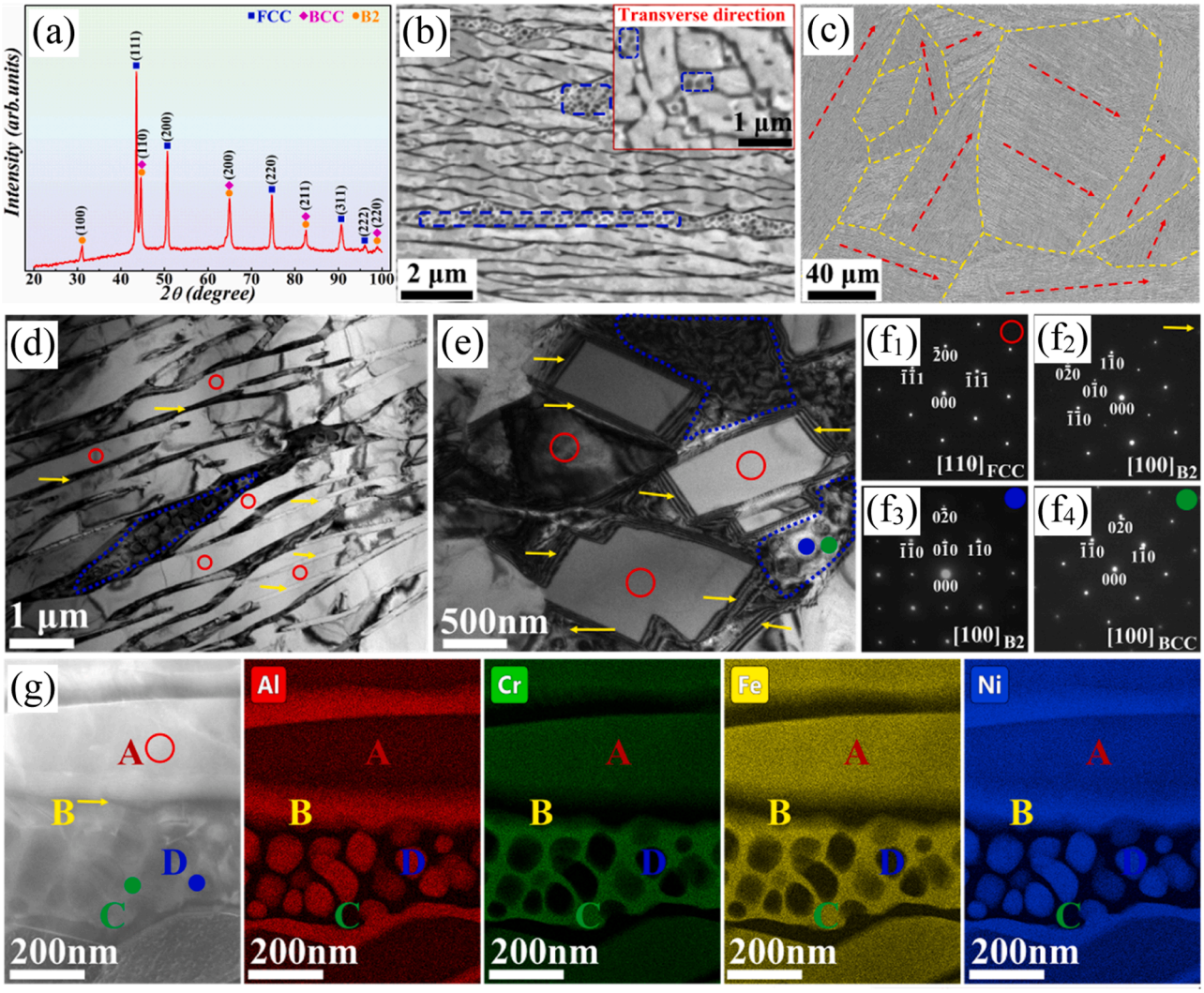

Fig. 1. Microstructure of the as-cast $FeNi_{0.9}Cr_{0.5}Al_{0.4}$ alloy. (a) XRD pattern, (b) representative high-magnification backscattered electron (BSE) image, the inset is magnified BSE image taken on perpendicular to the length of fibers, (c) low-magnification BSE image, (d) bright-field TEM image taken on parallel to the length of the fibers, (e) bright-field TEM image taken on perpendicular to the length of fibers, (f_1-f_4) SAED pattern of the fine fibers, fiber-shells, precipitates, and matrix of the secondary regions, (g) HAADF-STEM image and EDS elemental distribution maps of Al, Cr, Fe, Ni element.

rectangular dog-bone-shaped tensile samples with gauge length of ~10 mm, thickness of ~1.1 mm and width of ~2.7 mm were tested to confirm reproducibility.

The XRD pattern shown in Fig. 1(a) reveals that the as-cast $FeNi_{0.9}Cr_{0.5}Al_{0.4}$ alloy is primarily composed of a disordered FCC phase, a disordered BCC (A2) phase and an ordered BCC (B2) phase. The low-angle superlattice diffraction peak at 2θ values of ~30.9° is attributed to the (100) planes of the B2 phase, while the diffraction peaks of (110), (200), (211) and (220) overlap due to almost identical lattice parameters between A2 and B2 phases [9,11]. High-magnification BSE image in Fig. 1(b) shows that the predominant region of the as-cast $FeNi_{0.9}Cr_{0.5}Al_{0.4}$ alloy exhibits an interesting microstructure, consisting of dark thin longitudinal stripes and light thick layers. According to the distinct Z-contrast and XRD result, the stripes with dark contrast represent the Al-Ni-rich B2 phase, while the light layers with a dimension of dozens of micrometers in length are Al-depleted FCC phase, which will be identified by the following TEM analysis and EDS mapping. While observed along another crystallographic direction (the inset in Fig. 1b), the cross-section of the FCC layers shows a rectangle shape and the cross-sectional area is in the range of 0.6~1.7 μm^2, indicating that the FCC phase demonstrates a fiber-like morphology rather than a lamellar structure. Furthermore, the FCC fibers are encompassed on all four sides by the B2-structured shells. The thickness of B2 shells is lower than 100 nm, which is approximately a few one-tenth of B2 lamellae in typical lamellar-structured EHEAs ($\lambda \approx$ 1.1-2.3 μm) [10,11,21]. Additionally, it is worth noting that small amounts of secondary regions marked by the dashed blue circles, consisting of grey matrix and dark elliptical precipitates, can also be observed. Based on statistical analysis using ImageJ software, the volume fractions of the Al-depleted FCC fibers, B2 shells and secondary regions are estimated to be ~75.9 vol.%, ~9.8 vol.% and ~14.3 vol.% respectively. A further observation from the low-magnification BSE image presented in Fig. 1(c) and Fig. S1 suggest that the microstructure comprises near-equiaxed grains (enclosed by yellow dashed circles) with pronouncedly different fibrous orientations, displaying grain sizes of 50~250 μm. The crystallographic orientations of fibers within the grains are scattered with nearly parallel orientations (indicated by red dashed arrows).

Detailed TEM analyses were used to further identify the crystal structure and elemental distribution of $FeNi_{0.9}Cr_{0.5}Al_{0.4}$ alloy. Similarly, the bright-field image presented in Fig. 1(d) reveals the alternative structure of fine-scaled fibers (marked by red circles) and nano-sized fiber-shells (marked by yellow arrows) in the longitudinal direction. The TEM image corresponding to the transverse direction (Fig. 1e) shows that the fibers with an average cross-sectional area of ~1.3 μm^2 are enveloped in nano-sized shells with an average thickness of ~91 nm, further confirming the fibrous solidification microstructure. The selected area electron diffraction (SAED) pattern obtained from the fibers (Fig. 1f_1) exhibits the reflection of a disordered FCC structure, while the SAED pattern in Fig. 1(f_2) indicates that the shells have an ordered BCC (B2) structure. Meanwhile, the SAED patterns displayed in Fig. 1(f_3) and Fig. Fig. 1(f_4) show that the elliptical precipitates (marked by blue point) and matrix (marked by green point) of the secondary regions are ordered B2 and disordered BCC (A2) phases, respectively. High-angle annular dark-field scanning transmission electron microscope (HAADF-STEM) and EDS mapping were conducted to investigate the elemental distributions in this novel fibrous HEA. STEM-EDS maps and chemical compositions composed of all the phases are presented in Fig. 1 (g) and Table S1. According to the EDS results, the microstructure of $FeNi_{0.9}Cr_{0.5}Al_{0.4}$ alloy could be divided into four regions, i.e., FCC-structured fibers (labelled as A), B2-structured fiber-shells (labelled as B), A2-structured matrix of the secondary region (labelled as C), and B2-structured nano-precipitates (labelled as D). The EDS results reveal that the fibers are (Fe, Ni, Cr)-based FCC phase with some Al present, whereas the matrix of the secondary region is a Fe-Cr-rich phase, which is consistent with high contents of Cr and Fe favoring the formation of disordered BCC-structured phases in HEAs [21–23]. Furthermore, although the morphology varies greatly, the fiber-shells and elliptical precipitates have similar chemical compositions, i.e., enriched in Al and Ni. Specifically, the stoichiometry of shells and precipitates is described as $Ni_{50}(Al_{30}Fe_{15}Cr_5)_{50}$, which is a NiAl-like ordered phase with B2 structure [9,22-24]. The formation of this B2 intermetallic phase is promoted by the mixing enthalpy difference between sub-binary compounds in the FeNiCrAl HEAs system, most prominently, the highly negative enthalpy between Ni and Al [19]. These SEM and TEM observations confirm the premise that the solidification microstructure of the $FeNi_{0.9}Cr_{0.5}Al_{0.4}$ alloy exhibits a novel fibrous structure. For greater clarity, a schematic diagram of the microstructure of the $FeNi_{0.9}Cr_{0.5}Al_{0.4}$ HEA is illustrated in Fig. S2, showing that the fibrous heterogeneous structure, i.e., the (Fe, Ni, Cr)-based FCC-structured fine fibers (grey) are enveloped in Ni-Al-rich B2-structured nanosized fiber-shells (pink); in the meantime, there is a small amount of secondary region (~14.3 vol.%), showing that the disordered BCC matrix (yellow) contains B2 nanoprecipitates (pink).

Fig. 2(a) displays the typical uniaxial engineering tensile stress-strain curve (red line) of the as-cast $FeNi_{0.9}Cr_{0.5}Al_{0.4}$ specimen. Even without any microstructural homogenization or optimization, the alloy with fibrous microstructure exhibits a high yield strength ($\sigma_{0.2}$) of ~670 MPa and a remarkable ultimate tensile strength (σ_{UTS}) of ~1196 MPa with a large uniform elongation (ε_u) of ~21.1%, suggesting an excellent combination of tensile strength and ductility. The true stress (σ^t)-strain (ε^t) curve (blue line) was calculated based on the engineering stress-strain curve. The obtained true tensile yield, true ultimate tensile strength and true uniform elongation are ~676 MPa, ~1446 MPa and ~19.1%, respectively. These mechanical properties are directly related to the strain hardening rate (SHR) that is present during tensile deformation. The strain hardening rate ($d\sigma^t/d\varepsilon^t$) versus true strain curve (ε^t) displayed in Fig. 2(b) exhibits a typical three-stage strain hardening behavior with the increase of true strain, as generally observed in HEAs and conventional alloys [11,25-27]. The SHR first displays a significant drop from an ultra-high level in stage I ($\varepsilon^t < 3.5\%$), and then decreases steadily as the strain increases (stage II, $3.5\% < \varepsilon^t < 18.3\%$). In stage III ($18.3\% < \varepsilon^t$), the SHR decreases sharply upon tensile fracture. The stages of I and III with a dramatic SHR decline may be attributed to the dynamic recovery of dislocations and exhausted deformability, respectively [25]. In stage II, SHR slightly decreases from 6.1 GPa to 1.9 GPa in a wide strain range, mainly attributed to the serious hindering of dislocation movement by the abundant interfaces that are present between FCC-structured fibers and B2-structured shells.

To provide insight into the deformation and strengthening mechanisms that govern the behavior of the $FeNi_{0.9}Cr_{0.5}Al_{0.4}$ HEA, the strain-induced substructure evolution at different interrupted strains was investigated *via* TEM. After a relatively small true tensile strain of ~1.3% (~760 MPa), a few dislocations appeared in the soft FCC fibers, while no significant dislocation could be observed inside the hard B2 shells (Fig. 3a). Due to the different crystal structures, the soft FCC phase is more prone to initiating plastic deformation *via* the planar slip of the 1/2<110> dislocation on the {111} planes, whereas the dislocation in the B2 phase is difficult to nucleate and slip [25,28]. As the true strain was increased to ~3.5 % (~950 MPa), a dramatic increase in the dislocation density has been observed in the FCC fibers and massive dislocations pile-ups at the FCC/B2 interfaces, as marked by arrows in Fig. 3(b) and Fig. S3. The dislocation configuration within the FCC fibers exhibits the typical features of dislocation tangles caused by multi-slip and cross-slip, revealing strong interactions between dislocations [27, 28]. Simultaneously, the slip systems of the B2 structure were activated and a few dislocations could be observed in the B2 shells (Fig. 3b). Nevertheless, we have not observed appreciable planar dislocations inside the BCC/B2-structured secondary regions (Fig. 3c), suggesting that the hard BCC/B2 regions were still undergoing elastic deformation. The formation of hard BCC/B2 regions plays an important role in constraining the plastic deformation of the fiber-shell architecture. With further increases in the strain to fracture, high densities of dislocations

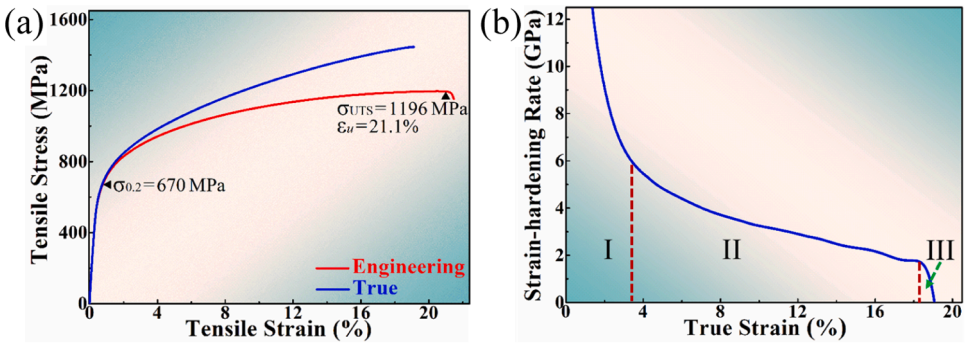

Fig. 2. Tensile properties of as-cast $FeNi_{0.9}Cr_{0.5}Al_{0.4}$ alloy at room temperature. (a) Representative uniaxial tensile stress-strain curves, (b) strain hardening rate ($d\sigma^t/d\varepsilon^t$) versus true strain (ε^t) curve.

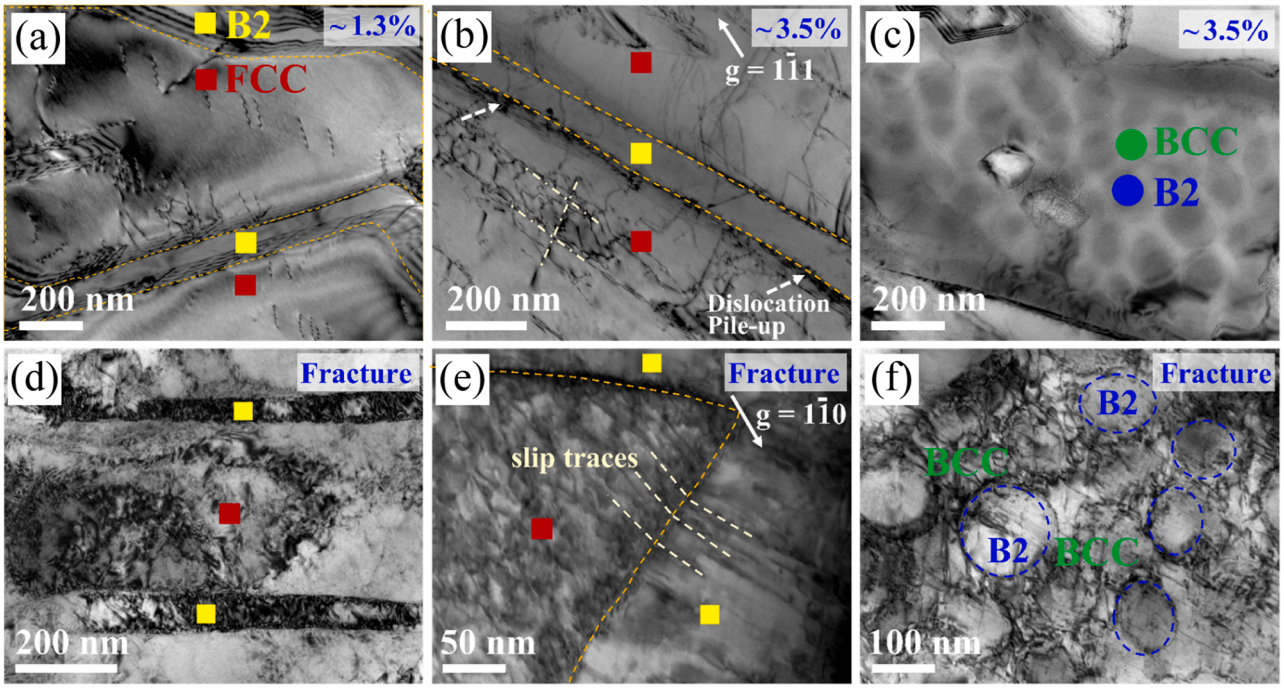

Fig. 3. TEM images of as-cast HEA at different strains. (a) Dislocation distribution of interrupted tensile specimen at true strain of ~1.3%, (b and c) dislocation distribution of interrupted tensile specimen at true strain of ~3.5%, (d-f) dislocation distribution of the fractured specimen.

were aggregated inside both FCC fibers and B2 shells (Fig. 3d), illustrating their superior dislocation storage capacity. Moreover, the slip traces traversing across the phase boundaries can be observed, as marked in Fig. 3(e), revealing that some of the accumulated dislocations at the interfaces could propagate to the B2 shells to release the stress concentration and achieve plastic co-deformation between FCC fibers and B2 shells, thereby rendering the as-cast $FeNi_{0.9}Cr_{0.5}Al_{0.4}$ HEA with high ductility. In addition to the predominant fibrous regions, quite a few of dislocations can also be observed in the BCC/B2 regions (Fig. 3f), indicating the emergence of plastic deformation and dislocations multiplication. Therefore, the heterostructured $FeNi_{0.9}Cr_{0.5}Al_{0.4}$ HEA consisted of three levels of regions with evidently different yield strength, i.e., FCC fibers, B2 shells and BCC/B2 secondary regions.

Recent studies have demonstrated that a critical advantage of heterogeneous structures is the strong hetero-deformation induced (HDI) hardening which originates from the generation of large local plastic strain gradients [18,21,28-31]. As shown in Fig. 3, plastic yielding initiated in the FCC fibers that possesses more slip systems, while the B2 shells and BCC/B2 regions deformed elastically. The geometrical constraints that are imposed by the still-elastically deforming phases, will lead to the formation of strong local plastic strain gradients near the high density of hetero-phase interfaces; these strain gradients are then accommodated *via* the build-up of geometrically necessary dislocations (GNDs) [21,29]. These GNDs interact with mobile dislocations and impede their motion, thereby generating an additional hardening mechanism which is described as HDI strengthening [18,29]. Moreover, after the B2 shells and BCC/B2 secondary regions deform plastically, an additional deformation incompatibility is generated between the co-deforming phases as a result of their different slip systems, and this is also accommodated by the formation of GNDs [32]. Consequently, the sustained pile-up of GNDs near the hetero-phase interfaces will generate strong HDI stresses, thereby increasing the overall flow stresses of the fibrous $FeNi_{0.9}Cr_{0.5}Al_{0.4}$ HEA [29,30]. To macroscopically calculate the magnitude of the HDI stress, we conducted Loading-Unloading-Reloading (LUR) tensile tests for the as-cast $FeNi_{0.9}Cr_{0.5}Al_{0.4}$ alloy and a typical LUR stress-strain curve is shown in Fig. 4(a). As evident from the figure, a large hysteresis loop appears in each LUR cycle, even near the yielding point, suggesting a strong Bauschinger effect and HDI hardening. The HDI stress can be calculated from LUR stress-strain curve as an average of unloading (σ_U) and

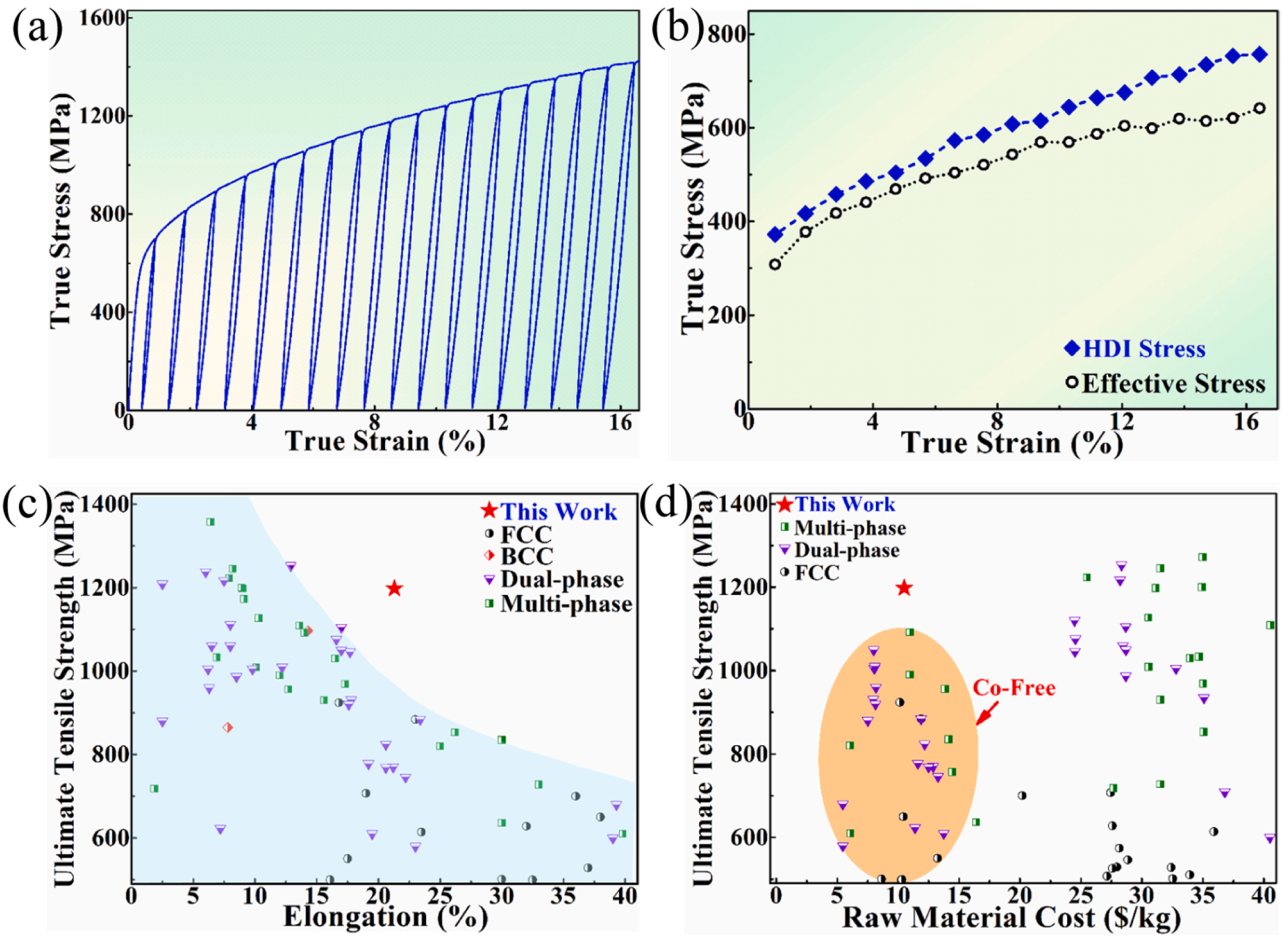

Fig. 4. (a) Loading-unloading-reloading (LUR) tensile stress-strain curve, (b) measured HDI stress and effective stress during deformation, (c) ultimate tensile strength versus elongation for the $FeNi_{0.9}Cr_{0.5}Al_{0.4}$ alloy in comparison with those as-cast HEAs reported in the literature, (d) ultimate tensile strength versus raw material cost for the $FeNi_{0.9}Cr_{0.5}Al_{0.4}$ alloy in comparison with those as-cast HEAs.

reloading (σ_R) yield stresses, namely, $\sigma_{HDI} = (\sigma_U + \sigma_R) / 2$ [31]. The detailed calculation methods for σ_U, σ_R and σ_{HDI} are summarized in references [31,32]. Additionally, the effective stress ($\sigma_{effetive}$) is acquired by subtracting the HDI stress from the flow stress (σ_{flow}), i.e., the stress induced by all other strengthening mechanisms except the HDI stress [32]. The calculation results of HDI stress and effective stress for the $FeNi_{0.9}Cr_{0.5}Al_{0.4}$ specimen during deformation are presented in Fig. 4 (b). The HDI stress contribution towards initial yield strength in the first LUR cycle is found to be ~372 MPa, and the HDI stress shows a monotonic increasing trend with the increase of applied strain. The evolution tendency of HDI stress and effective stress in $FeNi_{0.9}Cr_{0.5}Al_{0.4}$ alloy is similar to those of other reported heterostructured alloys [32–34]. The larger value of HDI stress in the $FeNi_{0.9}Cr_{0.5}Al_{0.4}$ alloy relative to that of the corresponding effective stress during the deformation, indicates that the contribution of HDI stress is higher than that of the effective stress. Therefore, these results suggest that the HDI hardening arising from fibrous heterogeneous structure is the primary strengthening mechanism for the as-cast $FeNi_{0.9}Cr_{0.5}Al_{0.4}$ HEA with a yield strength of ~670 MPa and an ultimate tensile strength of ~1196 MPa. Moreover, the HDI hardening also contributes to rendering the deformation more stable during tensile testing, which prevents the emergence of necking, and therefore promotes a high uniform elongation of ~21.1% [35].

To demonstrate the enhanced mechanical properties and reduced cost of the present alloy, we systematically compared the tensile properties and raw material cost of our developed fibrous heterogeneous HEA with those of reported HEAs fabricated by casting. The references and corresponding values are shown in Supplementary Table S2. According to the maps of ultimate tensile strength (σ_{UTS}) versus uniform elongation(ε_u) shown in Fig. 4(c), it is evident that the $FeNi_{0.9}Cr_{0.5}Al_{0.4}$ HEA, exhibiting an excellent combination of strength and ductility at ambient temperature, possesses a notable advantage relative to that of other reported as-cast HEAs. Additionally, Fig. 4(d) shows the comparison of raw materials cost between the $FeNi_{0.9}Cr_{0.5}Al_{0.4}$ HEA and other HEAs by the σ_{UTS}-cost scattergram. It is evident to found that the studied $FeNi_{0.9}Cr_{0.5}Al_{0.4}$ alloy marked with a red star is located at the upper-left area, indicating that the fibrous $FeNi_{0.9}Cr_{0.5}Al_{0.4}$ HEA get well along with the concept of cost-effective design and successfully achieve strength-cost synergy at ambient temperature.

To summarize, a novel Co-free $FeNi_{0.9}Cr_{0.5}Al_{0.4}$ HEA with a unique fibrous heterogeneous structure was successfully fabricated through the conventional arc-melting method. The dominant characteristic of $FeNi_{0.9}Cr_{0.5}Al_{0.4}$ alloy is the presence of nanoscale B2-structured hard shells that surround the comparatively soft fibers-like FCC phase. This fibrous heterostructured alloy possesses superior tensile properties with a yield strength of ~670 MPa, an ultimate tensile strength of ~1196 MPa and a uniform elongation of ~21.1%, respectively. This strength-ductility combination and superior work hardening ability are mainly attributed to HDI strengthening. These results are encouraging, suggesting that combining the conventional casting techniques with the HEAs concept may offer the opportunity to develop unusual microstructures that are rarely observed in traditional alloys, thereupon obtaining substantial performance improvement. Moreover, the alloy design strategy used in the current $FeNi_{0.9}Cr_{0.5}Al_{0.4}$ alloy also sheds light

on the development of low-cost yet strong alloys using simple casting techniques.

Declaration of competing interest

In the present work, we develop a novel Co-free non-equimolar $FeNi_{0.9}Cr_{0.5}Al_{0.4}$ HEA prepared by conventional arc melting. We observed that this HEA processes a unique fibrous heterogeneous solidification microstructure, i.e., fibers-like FCC soft phases that are enveloped in nano-sized B2 hard shells. This fibrous microstructure is thought to be responsible for the notable mechanical properties, which includes an ultimate tensile strength of ~1196 MPa, together with a uniform elongation of ~21.1% at room temperature. Experimental results confirm the suggestion that the combination of a high tensile strength and good ductility can be attributed to the hetero-deformation induced hardening mechanism generated from the soft-fiber and hard-shell interface.

The authors declare that they have no known competing financial interests or personal relationships that could have appeared to influence the work reported in this paper.

Acknowledgements

The authors acknowledge the financial support by the Key-Area Research and Development Program of Guangdong Province (Grant No. 2018B090905002), National Natural Science Foundation of China (Grant No. 52103360), and China Scholarship Council (Grant No. 201906150074). The experimental support of the Karlsruhe Nano Micro Facility (KNMF), a Helmholtz Research Infrastructure at Karlsruhe Institute of Technology is gratefully acknowledged. The authors also thank the technical support of Sinoma Institute of Materials Research (Guang Zhou) Co., Ltd.

References

[1] S. Pattnaik, D.B. Karunakar, P.K. Jha, Developments in investment casting process-a review, J. Mater. Process. Technol. 212 (2012) 2332–2348.
[2] Z. Niu, G. Liu, T. Li, S. Ji, Effect of high pressure die casting on the castability, defects and mechanical properties of aluminium alloys in extra-large thin-wall castings, J. Mater. Process. Technol. 303 (2022), 117525.
[3] J.W. Yeh, S.K. Chen, S.J. Lin, J.Y. Gan, T.S. Chin, T.T. Shun, C.H. Tsau, S.Y. Chang, Nanostructured high-entropy alloys with multiple principal elements: novel alloy design concepts and outcomes, Adv. Eng. Mater. 6 (2004) 299–303.
[4] B. Cantor, I.T.H. Chang, P. Knight, A.J.B. Vincent, Microstructural development in equiatomic multicomponent alloys, Mater. Sci. Eng. A 375–377 (2004) 213–218.
[5] Z. Fu, L. Jiang, J.L. Wardini, B.E. MacDonald, H. Wen, W. Xiong, D. Zhang, Y. Zhou, T.J. Rupert, W. Chen, E.J. Lavernia, A high-entropy alloy with hierarchical nanoprecipitates and ultrahigh strength, Sci. Adv. 4 (2018) 1–9.
[6] Y. Lu, A. Mazilkin, T. Boll, N. Stepanov, S. Zherebtzov, G. Salishchev, É. Ódor, T. Ungar, E. Lavernia, H. Hahn, Y. Ivanisenko, Influence of carbon on the mechanical behavior and microstructure evolution of CoCrFeMnNi processed by high pressure torsion, Materialia 16 (2021), 101059.
[7] S. Peng, S. Mooraj, R. Feng, L. Liu, J. Ren, Y. Liu, F. Kong, Z. Xiao, C. Zhu, P. K. Liaw, W. Chen, Additive manufacturing of three-dimensional (3D)-architected CoCrFeNiMn high-entropy alloy with great energy absorption, Scr. Mater. 190 (2021) 46–51.
[8] G. Qin, R. Chen, P.K. Liaw, Y. Gao, L. Wang, Y. Su, H. Ding, J. Guo, X. Li, An as-cast high-entropy alloy with remarkable mechanical properties strengthened by nanometer precipitates, Nanoscale 12 (2020) 3965–3976.
[9] Z. Jiang, W. Chen, Z. Xia, W. Xiong, Z. Fu, Influence of synthesis method on microstructure and mechanical behavior of Co-free AlCrFeNi medium-entropy alloy, Intermetallics 108 (2019) 45–54.
[10] Y. Lu, Y. Dong, S. Guo, L. Jiang, H. Kang, T. Wang, B. Wen, Z. Wang, J. Jie, Z. Cao, H. Ruan, T. Li, A promising new class of high-temperature alloys: eutectic high-entropy alloys, Sci. Rep. 4 (2014) 1–5.
[11] P. Shi, W. Ren, T. Zheng, Z. Ren, X. Hou, J. Peng, P. Hu, Y. Gao, Y. Zhong, P. K. Liaw, Enhanced strength–ductility synergy in ultrafine-grained eutectic high-entropy alloys by inheriting microstructural lamellae, Nat. Commun. 10 (2019) 1–8.
[12] Y. Yin, A. Atrens, H. Huang, X.M. Zhang, Cost-Effective Fe-Rich High-Entropy Alloys: A Brief Review, IntechOpen, London, 2022.
[13] Y. Yin, J. Zhang, Q. Tan, W. Zhuang, N. Mo, M. Bermingham, M.X. Zhang, Novel cost-effective Fe-based high entropy alloys with balanced strength and ductility, Mater. Des. 162 (2019) 24–33.
[14] M. Zhang, Y. Ma, W. Dong, X. Liu, Y. Lu, Y. Zhang, R. Li, Y. Wang, P. Yu, Y. Gao, G. Li, Phase evolution, microstructure, and mechanical behaviors of the $CrFeNiAl_xTi_y$ medium-entropy alloys, Mater. Sci. Eng. A 771 (2020).
[15] Z. Li, K.G. Pradeep, Y. Deng, D. Raabe, C.C. Tasan, Metastable high-entropy dual-phase alloys overcome the strength–ductility trade-off, Nature 534 (2016) 227–230.
[16] Y. Yin, Q. Tan, Q. Sun, W. Ren, J. Zhang, S. Liu, Y. Liu, M. Bermingham, H. Chen, M.X. Zhang, Heterogeneous lamella design to tune the mechanical behaviour of a new cost-effective compositionally complicated alloy, J. Mater. Sci. Technol. 96 (2022) 113–125.
[17] F. He, Z. Wang, C. Ai, J. Li, J. Wang, J.J. Kai, Grouping strategy in eutectic multi-principal-component alloys, Mater. Chem. Phys. 221 (2019) 138–143.
[18] Y. Lu, H. Jiang, S. Guo, T. Wang, Z. Cao, T. Li, A new strategy to design eutectic high-entropy alloys using mixing enthalpy, Intermetallics 91 (2017) 124–128.
[19] A. Takeuchi, A. Inoue, Classification of bulk metallic glasses by atomic size difference, heat of mixing and period of constituent elements and its application to characterization of the main alloying element, Mater. Trans. 46 (12) (2005) 2817–2829.
[20] C. Li, Y. Wu, H. Li, Y. Wu, X. Liu, Effect of Ni on eutectic structural evolution in hypereutectic Al–Mg2Si cast alloys, Mater. Sci. Eng. A 528 (2010) 573–577.
[21] P. Shi, Y. Zhong, Y. Li, W. Ren, T. Zheng, Z. Shen, B. Yang, J. Peng, P. Hu, Y. Zhang, P.K. Liaw, Y. Zhu, Multistage work hardening assisted by multi-type twinning in ultrafine-grained heterostructural eutectic high-entropy alloys, Mater. Today 41 (2020) 62–71.
[22] R.S. Ganji, P. Sai Karthik, K. Bhanu Sankara Rao, K.V. Rajulapati, Strengthening mechanisms in equiatomic ultrafine grained AlCoCrCuFeNi high-entropy alloy studied by micro-and nanoindentation methods, Acta Mater 125 (2017) 58–68.
[23] K. Srimark, S. Dasari, A. Sharma, P. Wangyao, B. Gwalani, T. Rojhirunsakool, S. Gorsse, R. Banerjee, Hierarchical phase evolution in a lamellar $Al_{0.7}CoCrFeNi$ high entropy alloy involving competing metastable and stable phases, Scr. Mater. 204 (2021), 114137.
[24] Z. Jiang, W. Chen, T. Cheng, Z. Fu, S. Peng, S. Guan, As-cast Co-free $Al_{0.4}Ni_{0.4}CrFe$ high entropy alloy with hierarchical coherent precipitates and remarkable mechanical properties, Mater. Today Commun. 35 (2023), 105565.
[25] H. Jiang, D.X. Qiao, W.N. Jiao, K.M. Han, Y.P. Lu, P.K. Liaw, Tensile deformation behavior and mechanical properties of a bulk cast Al0. 9CoFeNi2 eutectic high-entropy alloy, J. Mater. Sci. Technol. 61 (2021) 119–124.
[26] Z. Zhang, Z. Jiang, Y. Xie, S.L.I. Chan, J. Liang, J. Wang, Multiple deformation mechanisms induced by pre-twinning in CoCrFeNi high entropy alloy, Scr. Mater. 207 (2022), 114266.
[27] L. Zhang, R. Song, C. Zhao, F. Yang, Y. Xu, S. Peng, Evolution of the microstructure and mechanical properties of an austenite–ferrite Fe–Mn–Al–C steel, Mater. Sci. Eng. A 643 (2015) 183–193.
[28] T. Xiong, W. Yang, S. Zheng, Z. Liu, Y. Lu, R. Zhang, Y. Zhou, X. Shao, B. Zhang, J. Wang, F. Yin, P.K. Liaw, X. Ma, Faceted Kurdjumov-Sachs interface-induced slip continuity in the eutectic high-entropy alloy, $AlCoCrFeNi_{2.1}$, J. Mater. Sci. Technol. 65 (2021) 216–227.
[29] Y. Zhu, K. Ameyama, P.M. Anderson, I.J. Beyerlein, H. Gao, H.S. Kim, E. Lavernia, S. Mathaudhu, H. Mughrabi, R.O. Ritchie, N. Tsuji, X. Zhang, X. Wu, Heterostructured materials: superior properties from hetero-zone interaction, Mater. Res. Lett. 9 (2021) 1–31.
[30] Y.F. Wang, C.X. Huang, X.T. Fang, H.W. Höppel, M. Göken, Y.T. Zhu, Hetero-deformation induced (HDI) hardening does not increase linearly with strain gradient, Scr. Mater. 174 (2020) 19–23.
[31] M. Yang, Y. Pan, F. Yuan, Y. Zhu, X. Wu, Back stress strengthening and strain hardening in gradient structure, Mater. Res. Lett. 4 (2016) 145–151.
[32] J. Moon, J.M. Park, J.W. Bae, N. Kang, J. Oh, H. Shin, H.S. Kim, Hetero-deformation-induced strengthening by twin-mediated martensitic transformation in an immiscible medium-entropy alloy, Scr. Mater. 186 (2020) 24–28.
[33] W. Lu, X. Luo, D. Ning, M. Wang, C. Yang, M. Li, Y. Yang, P. Li, B. Huang, Excellent strength-ductility synergy properties of gradient nano-grained structural CrCoNi medium-entropy alloy, J. Mater. Sci. Technol. 112 (2022) 195–201.
[34] Y. Zou, H. Ding, Y. Zhang, Z. Tang, Microstructural evolution and strain hardening behavior of a novel two-stage warm rolled ultra-high strength medium Mn steel with heterogeneous structures, Int. J. Plast. 151 (2022), 103212.
[35] X. Wu, Y. Zhu, Heterogeneous materials: a new class of materials with unprecedented mechanical properties, Mater. Res. Lett. 5 (2017) 527–532.